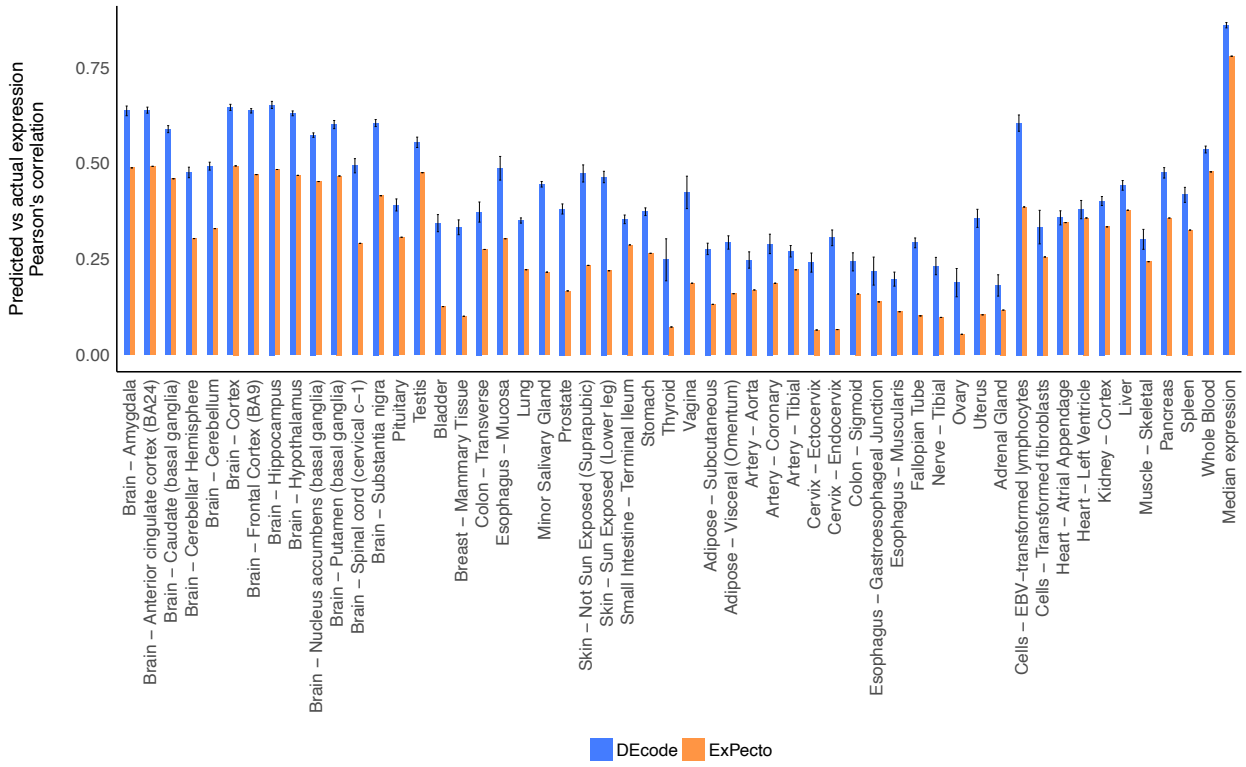

Supplementary Figure 1. Performance comparison of DEcode with ExPecto with respect to correlation coefficient.

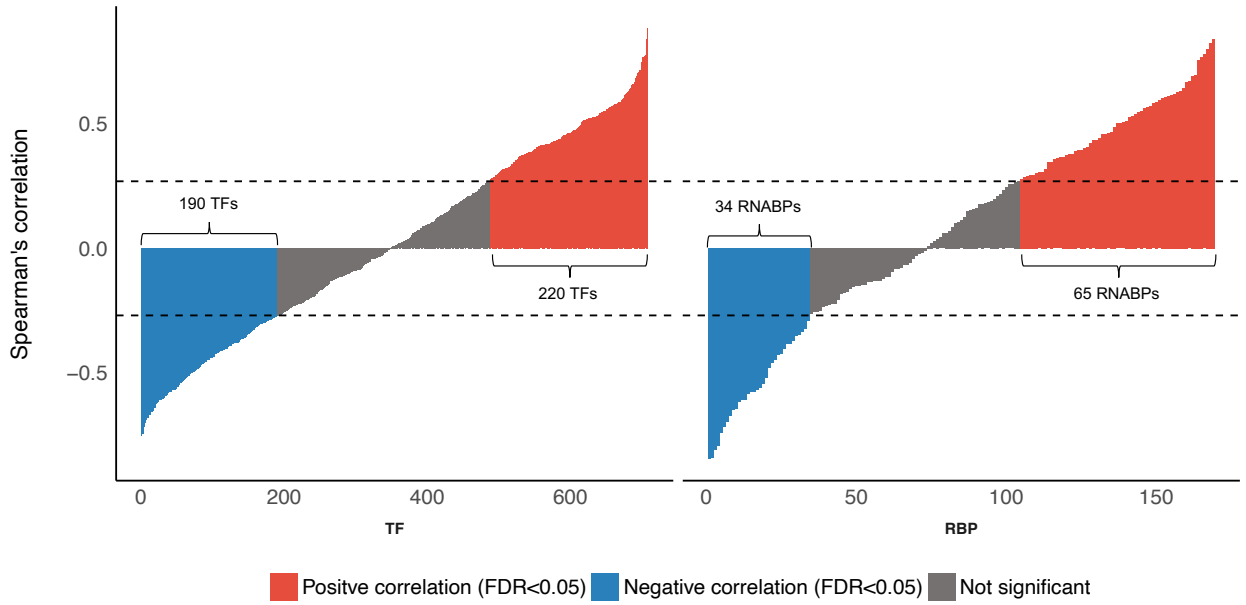

Supplementary Figure 2. Correlation between DeepLIFT scores vs log2-TPMs for each of TFs and RNABPs. Spearman's correlation was used to evaluate the relation between DeepLIFT scores vs log2-TPMs. The Benjamini–Hochberg procedure was used to control the false discovery rate at 5%.

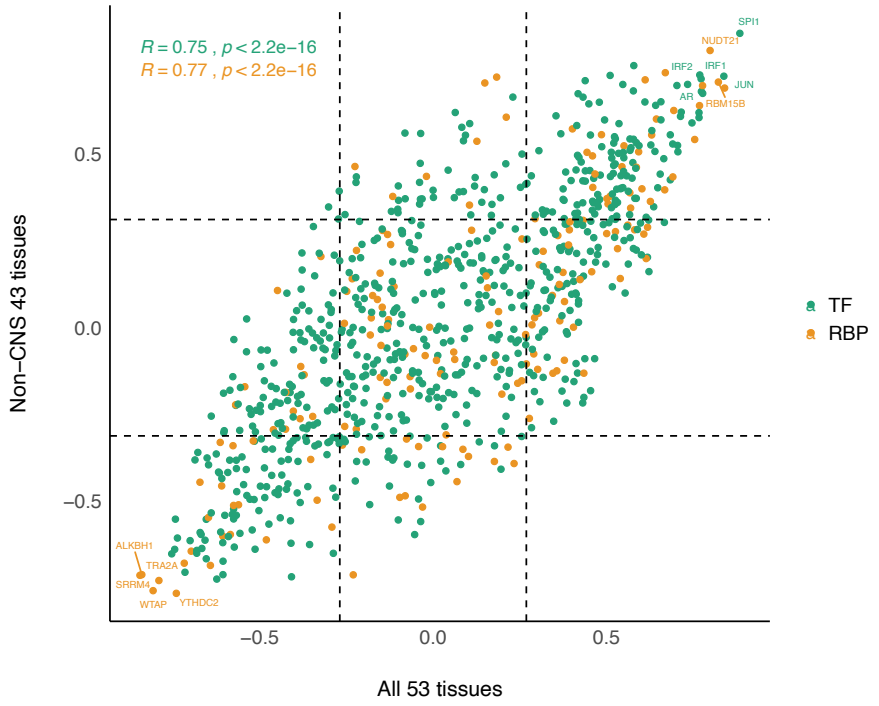

Supplementary Figure 3. Relationships of regulators' DeepLIFT scores with their log2-TPMs with or without brain tissues. Spearman's correlations between DeepLIFT scores vs log2-TPMs for each of TFs and RNABPs were computed using all 53 tissues and 43 tissues without brain tissues, respectively. The Spearman's correlations from the two sets of tissues were contrasted by a scatter plot.

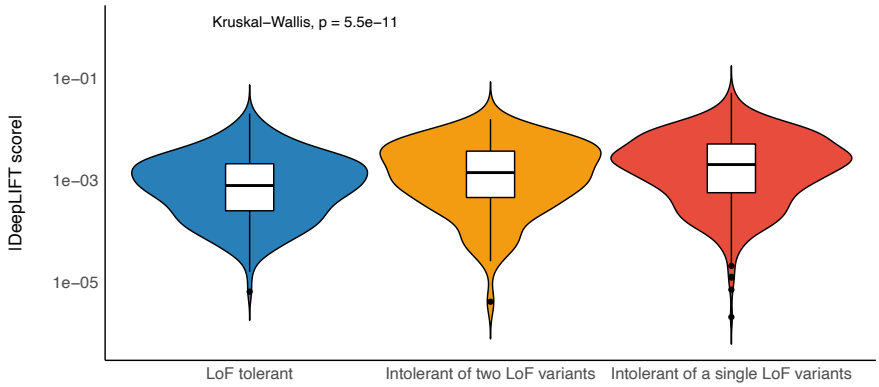

Supplementary Figure 4. The overlap between the key regulators for the median absolute expression levels and LoF intolerant genes. The LoF intolerant genes were split into genes intolerant to heterozygous LoF mutations and genes intolerant to homozygous LoF mutations.

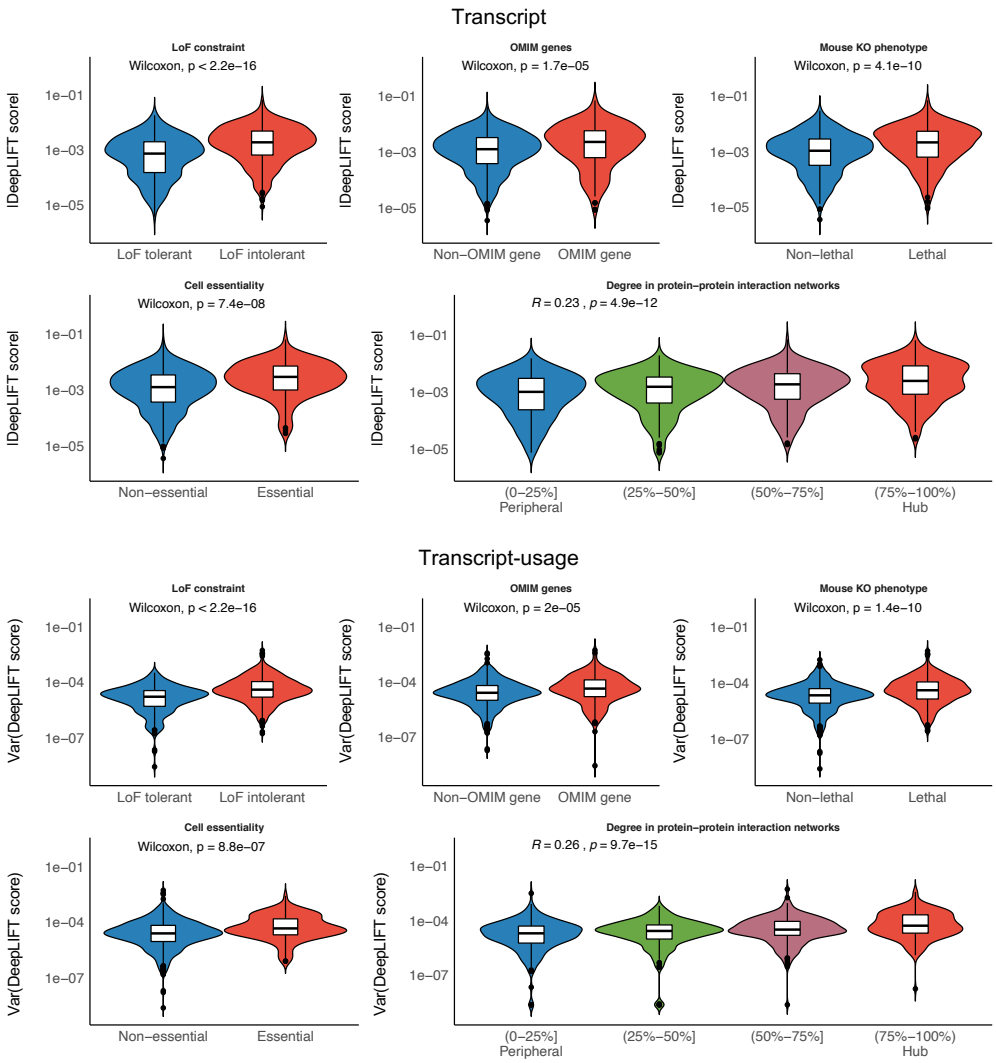

Supplementary Figure 5. The overlap between the key regulators for the fold-change across 53 tissues in the transcript-based model and external functional gene sets.

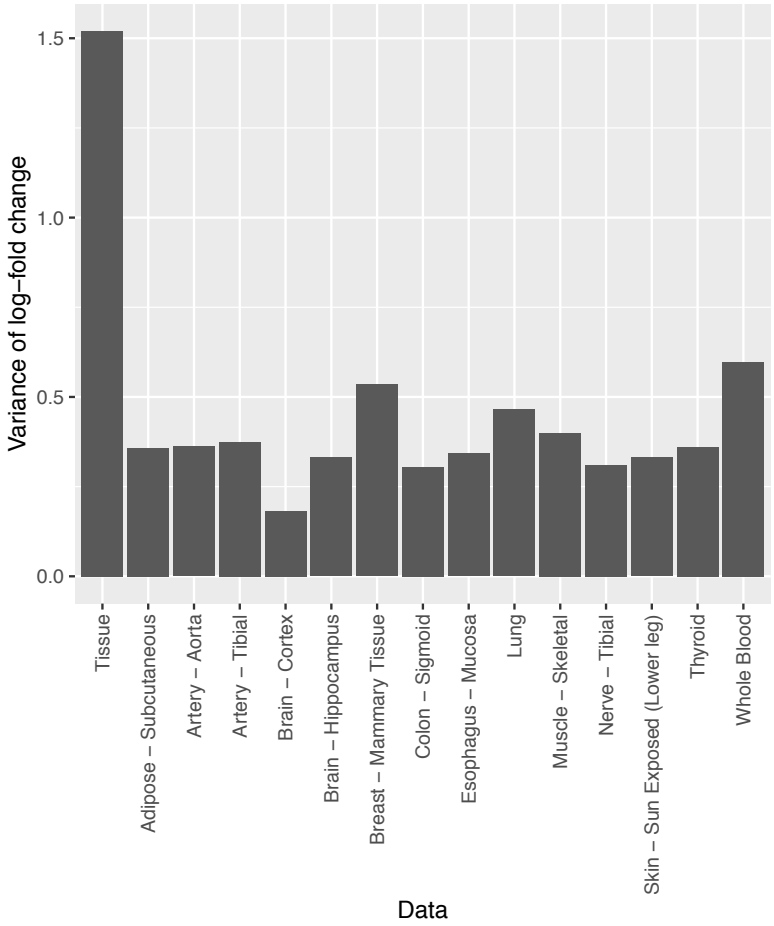

Supplementary Figure 6. The variance of gene expression between tissues and within tissues. We computed variances in log-fold changes based on mean TPMs across 53 tissues and those based on TPMs across individuals in each tissue.

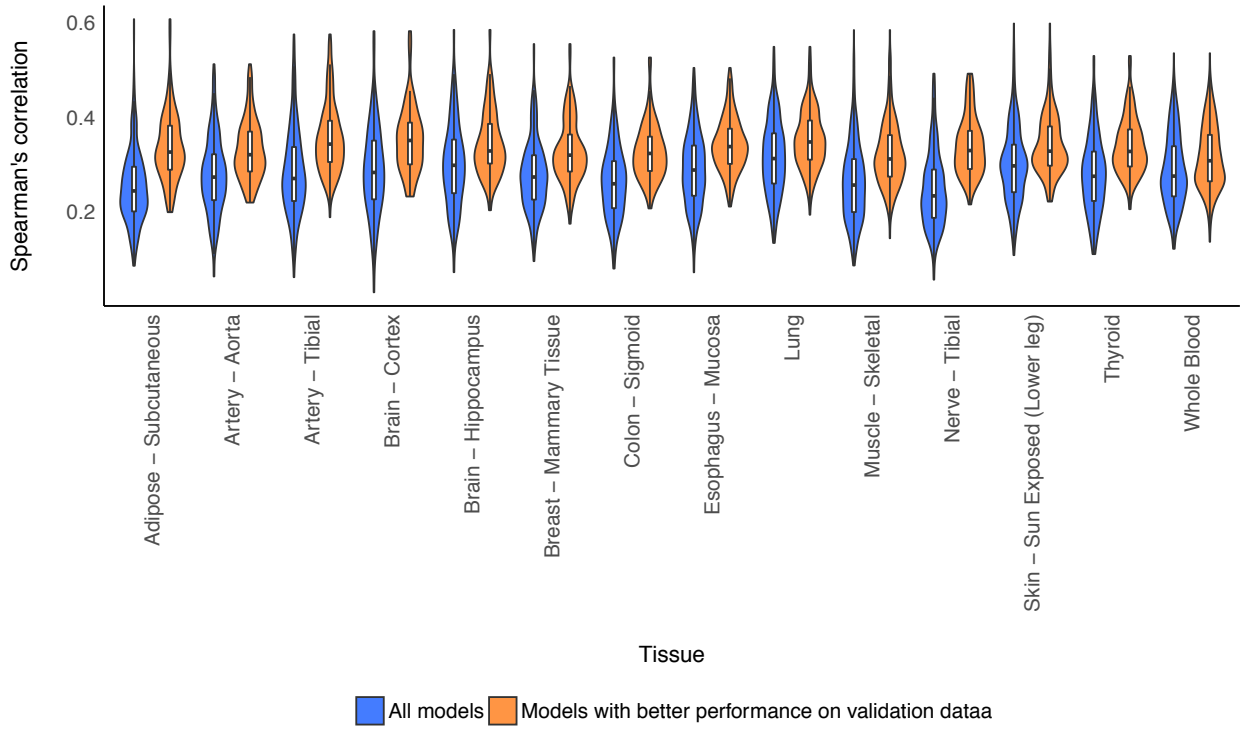

Supplementary Figure 7. The predictive performances of the person-specific models. We computed Spearman's correlation between the predicted gene expression and the actual gene expression for each individual. We filtered out person-specific predictions from the models whose performances on validation data were less than 50% percentile of all individuals in each tissue.

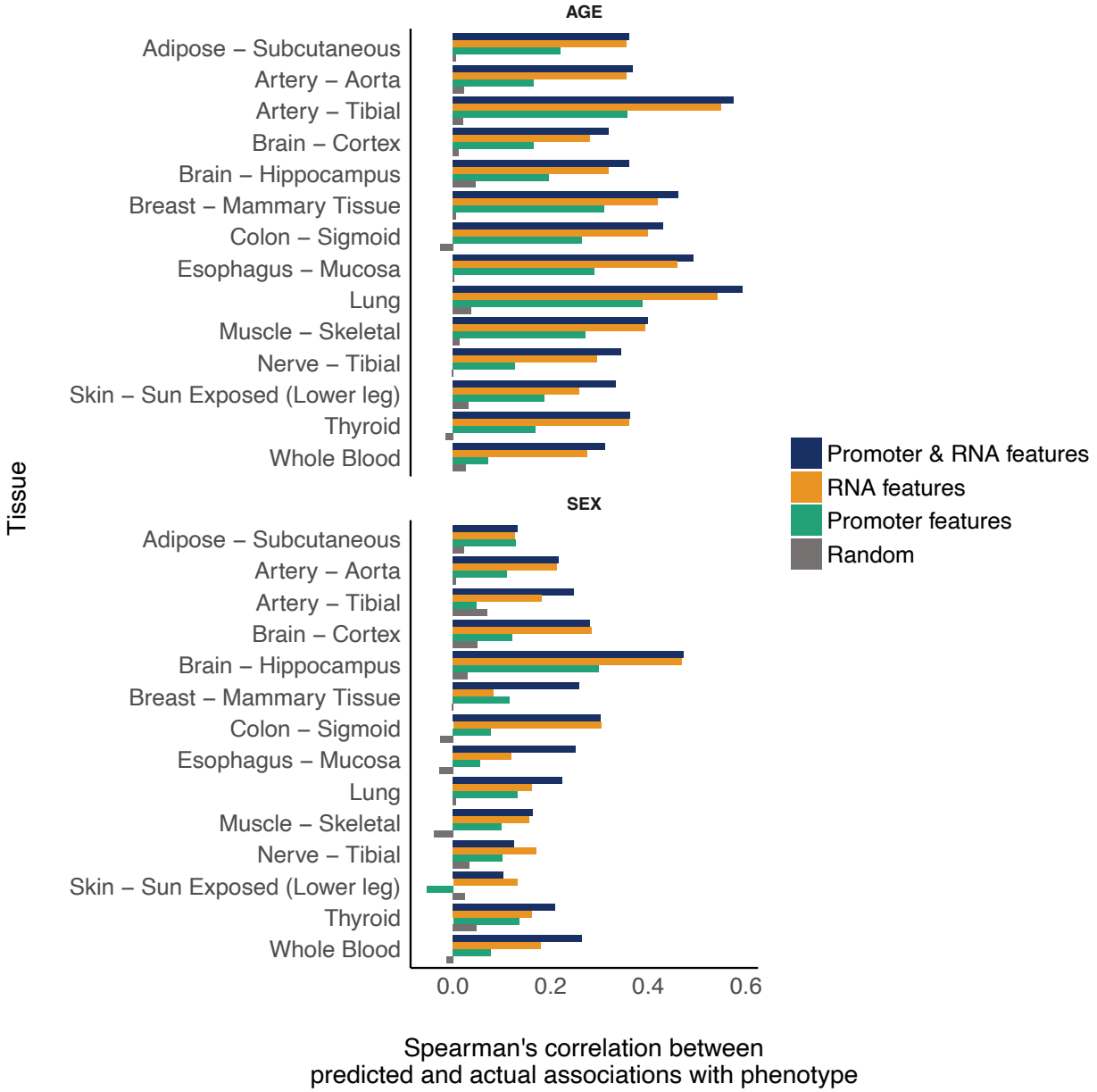

Supplementary Figure 8. Comparison of performances in predicting phenotype-associated DEs with a distinct feature set. The bar plots show Spearman's correlation between t-statistics of DE using the predicted and the actual gene expression.

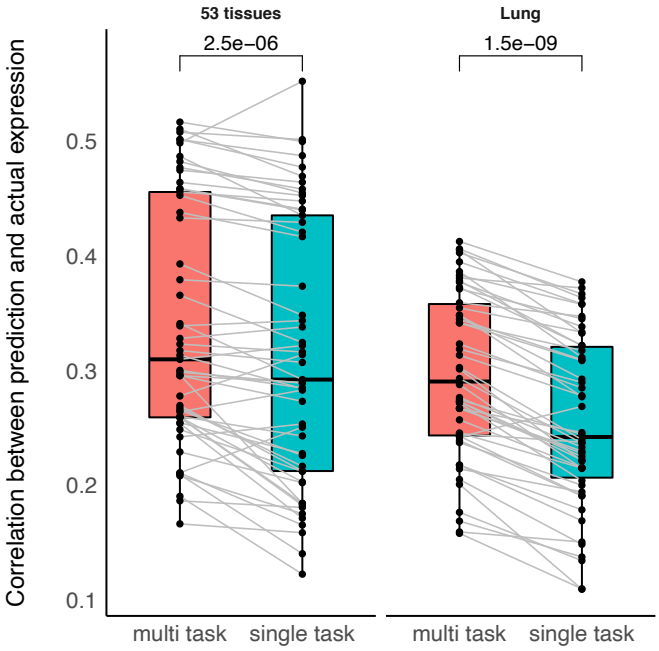

Supplementary Figure 9. Comparison of the multi-task model with the single-task model. Boxplots contrasts predictive performance of the multi-task model with the single-task model for the fold-change across 53 tissues and randomly selected 50 lung samples. The paired sample t-test was used to assess the statistical significance of the differential performance.

Gene model

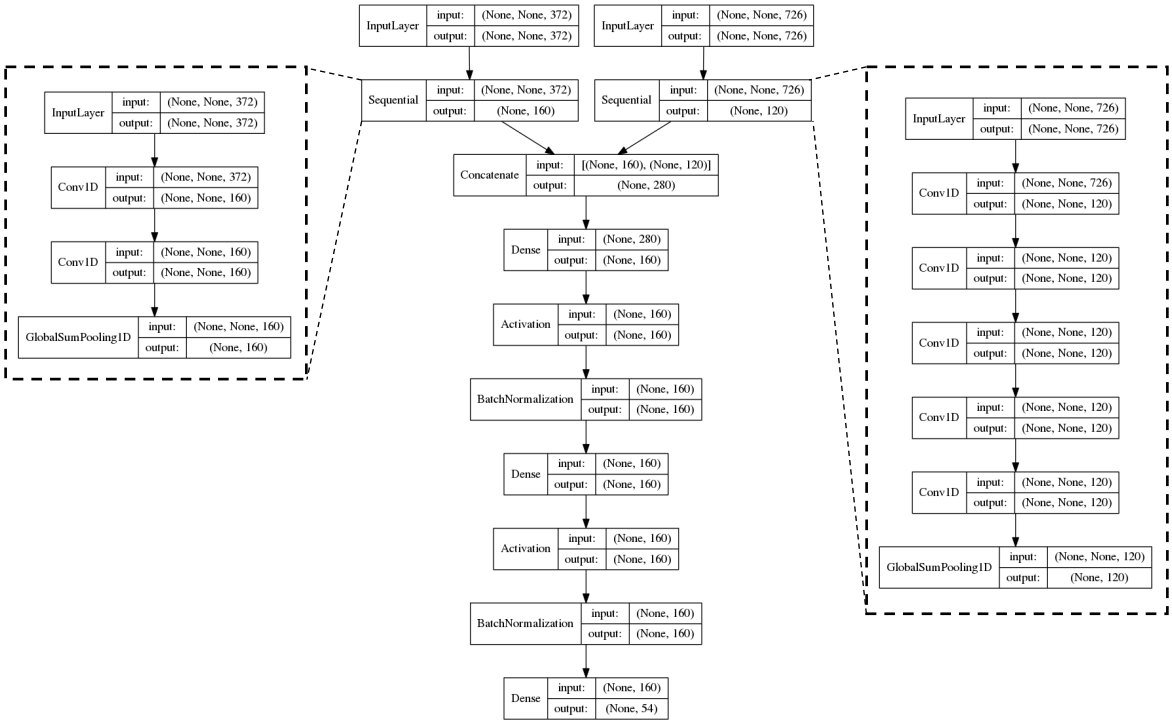

Transcript model

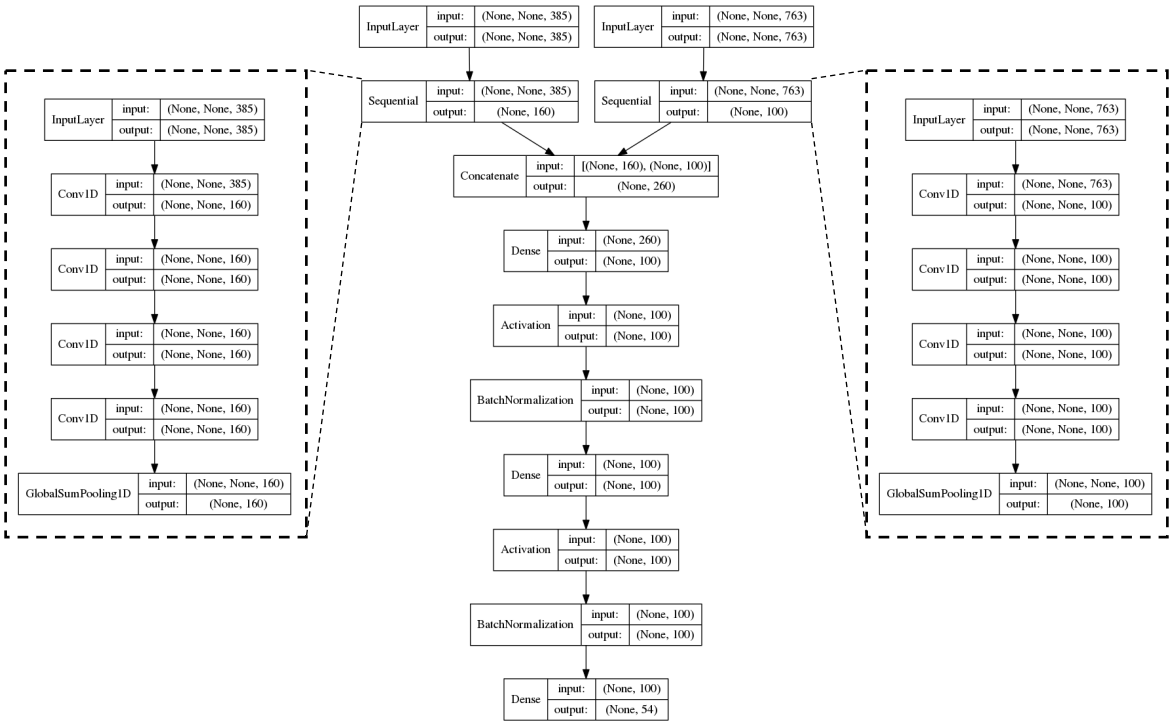

Supplementary Figure 10. Structures of deep neural networks in DEcode.

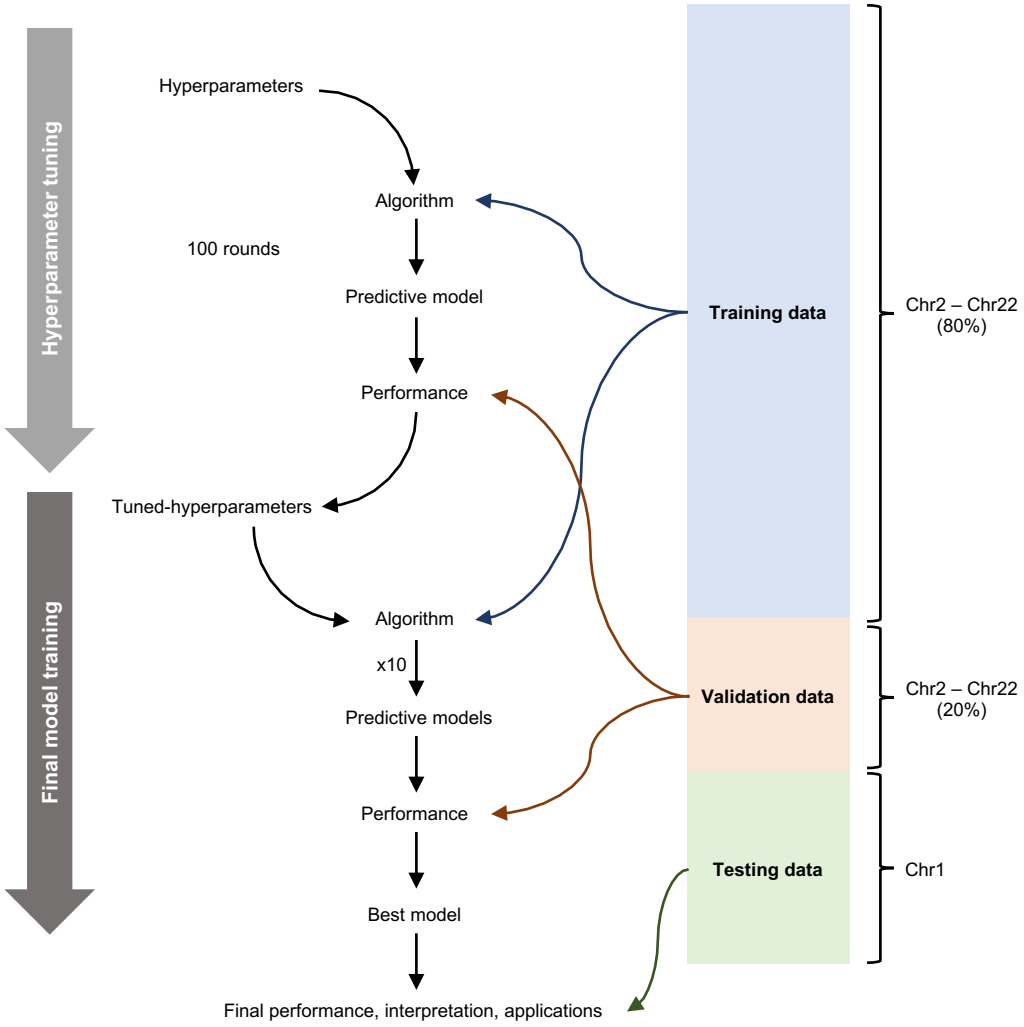

Supplementary Figure 11. Overview of DEcode model building pipeline for tissue-specific expression.

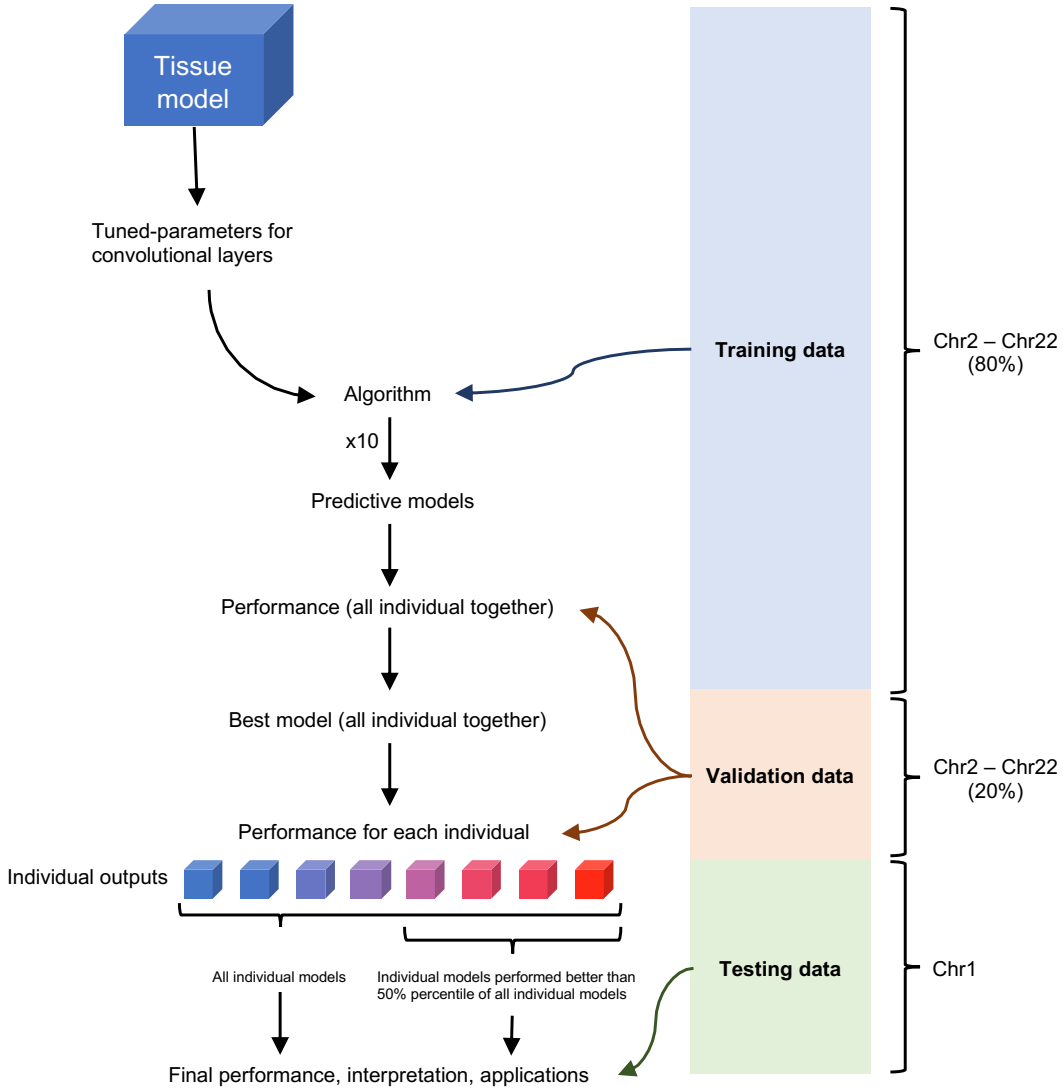

Supplementary Figure 12. Overview of DEcode model building pipeline for person-specific expression.